Drift current induced tunable spin current in inverted-graphene based spin valve

Carbon 237 (2025) 120140

Contents lists available at ScienceDirect

Carbon

journal homepage: www.elsevier.com/locate/carbon

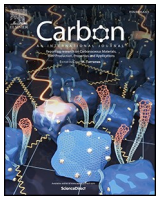

Drift current induced tunable spin current in inverted-graphene based spin valve

Jian Zhou [a,b], Xianyang Lu [a,c,*], Bing Zhao [d], Jiaju Yang [e], Yu Yan [a,b], Jing Wu [f], Yong Pu [e], Rong Zhang [b], Yongbing Xu [a,b,c,f,**]

[a] National Key Laboratory of Spintronics, Nanjing University, Suzhou, 215163, China
[b] Jiangsu Provincial Key Laboratory of Advanced Photonic and Electronic Materials, School of Electronic Science and Engineering, Nanjing University, Nanjing, 210093, China
[c] School of Integrated Circuits, Nanjing University, Suzhou, 215163, China
[d] Department of Microtechnology and Nanoscience, Chalmers University of Technology, SE-41296, Göteborg, Sweden
[e] College of Science, Nanjing University of Posts and Telecommunications (NJUPT), Nanjing, 210023, China
[f] York-Nanjing International Joint Center in Spintronics, Department of Electronics and Physics, University of York, York, YO10 5DD, UK

ARTICLE INFO

Keywords:
Inverted-graphene spin valve
Spin current and electrical current
Nonlinear bias dependence
Drift current effect

ABSTRACT

Understanding the interplay between electrical current and spin current in graphene is crucial for the realization of the potential of the graphene-based spintronic devices. In this work, we investigate spin transport under both bias (the DC current applied within an injection circuit) and external currents (applied beyond the injection circuit), emphasizing the pivotal role of the drift field, in the inverted graphene-based spin valve. We discover that the spin current can be effectively tuned with electrical current, exhibiting notable differences at various gate voltages. Further Hanle measurements confirm that external electrical current not only tunes the spin diffusion current but also simultaneously enhances the spin-injection polarization. We observe a strong nonlinear bias behavior, particularly with a reversal of the sign of the spin signal at negative bias currents, demonstrating the spin drift effect. These findings underscore the importance of drift current in affecting spin transport in the graphene-based spin devices.

1. Introduction

In spintronics, the efficient generation, manipulation, and detection of spin currents are crucial for developing next-generation electronic devices [1–3]. Spin currents, which carry spin angular momentum, can be manipulated through various means, including magnetic fields, spin-orbit coupling, and electrical currents [4–6]. Among these, using electrical currents to control spin signals offers a direct and efficient method for integrating spintronic functionalities into conventional electronic circuits [7–10]. Non-local spin valves can separating spin and charge currents, providing an efficient way to study the impact of charge currents on spin currents [11–14]. In our previous work, we introduced an all-dry van der Waals transfer method to create a clean and solvent-free graphene-based lateral spin-valve device, where a long spin lifetime was observed. We have further found that the intrinsic spin transport of the contamination-free graphene-based spin valve has an abnormal temperature dependence [15]. The contamination-free device can also effectively reduce spin dephasing caused by invasive contact and phonon scattering due to the substrate and polluted graphene [16–18]. These advantages make the contamination-free graphene-based spin valve an excellent medium for studying the interplay between electrical current and spin current as in this work.

For the practical implementation of future spintronic devices, especially in seamlessly integrating memory and spin-logic circuits at room temperature [19–23], it becomes crucial to manipulate spin signals electrically. A deeper understanding of the intrinsic connection between spin currents and charge currents is essential for achieving this goal. Extensive experiments have been conducted to manipulate spin transport in graphene through electrical currents [24–29]. The application of external current beyond the injection circuit effectively modulates the spin signal by creating an in-plane transverse external electrical field, typically influencing the spin diffusion process [30,31]. However, the

* Corresponding author. School of Integrated Circuits, Nanjing University, Suzhou, 215163, China.
** Corresponding author. National Key Laboratory of Spintronics, Nanjing University, Suzhou, 215163, China.
E-mail addresses: xylu@nju.edu.cn (X. Lu), ybxu@nju.edu.cn (Y. Xu).

https://doi.org/10.1016/j.carbon.2025.120140
Received 29 June 2024; Received in revised form 26 January 2025; Accepted 19 February 2025
Available online 20 February 2025

impact of external DC current on the spin injection process remains incompletely understood. Specifically, it remains to be determined whether such external currents affect the creation of the spin current (spin injection polarization) similarly to the local DC bias current applied within the injection circuit. Previous studies have shown that local DC bias current can significantly influence spin injection efficiency [32–36]. Understanding the impact of external current on spin injection and diffusion is crucial for gaining insights into the mechanisms underlying spin currents influenced by electric fields. Notably, Hanle precession measurements provide an effective means to extract spin transport-related parameters. Therefore, a systematic investigation of the relationship between external DC current and spin transport-related parameters is needed.

In this work, we investigate the tunability of the spin currents in the inverted graphene-based spin valve (IGSV) using electrical current. We studied the spin signal's response under different gate voltages and observed that the in-plane electrical field plays a crucial role in both the spin diffusion and spin injection processes, as evidenced by Hanle precession measurements. Additionally, we observed a nonlinear bias dependence with a sign reversal occurring at a negative DC bias. Through further analysis of this sign reversal under bias current, we compared it with several mechanisms and found that the drift field effect combined with the pinhole model in our device plays a significant role in this nonlinear bias dependence behavior.

2. Experimental details

The device fabrication process involves two main steps. Firstly, Co (40 nm)/Ti (0.5 nm) electrodes are prepared on a 280 nm SiO_2/Si substrate using electron-beam lithography (EBL) to define the size of the electrode and using the electron beam evaporator (EBE) to evaporate material. The widths of the injector and detector ferromagnetic electrodes are approximately 2 μm and 1 μm, respectively. The second step is to transfer the single-layer graphene (SLG) onto the prepared electrodes. We use a PDMS/hBN stack to pick up SLG on the SiO_2 substrate. After SLG is successfully transferred from the substrate, the hBN/SLG heterostructure is placed on the prepared electrodes. All transfer processes are carried out without any solvent assistance to maintain a clean interface between graphene and electrode. A back gate voltage is applied to the Si substrate to tune the carrier concentration in graphene.

The illustrations of the nonlocal spin transport measurement are shown in Fig. 1(a). An AC current (I_{AC}) is applied to the left circuit (contact 1 and 2) as a spin injection source, while the nonlocal voltage (V_{NL}) is measured in the right circuit using a standard low-frequency lock-in technique at 13 Hz. In nonlocal measurements, after the charge current is injected from the injector, the resulting spin accumulation diffuses away, creating a spin current. The ferromagnetic detector electrode measures this spin accumulation by detecting the nonlocal voltage V_{NL}, which represents the magnitude of the spin current [37–39]. The in-plane magnetic field (B_y) is applied along the easy axis of the magnetic electrode (y-axes), and the nonlocal resistance is determined by $R_{NL} = V_{NL}/I_{AC}$. The bias current (I_{Bias}) is applied between the left circuit in contact 1 and 2, while the external current (I_{Ext}) is applied between contact 1 and 3. The nonmagnetic electrode (contact 3) is positioned between the injector and the detector, which could absorb spin current and lead to a reduction in the spin signal [40].

3. Results and discussion

The typical nonlocal resistance as a function of an in-plane magnetic field is shown in Fig. 1(b). The green arrow represents the magnetization direction of injection ferromagnetic electrode (contact 4), while the blue and red curves represent the trace of the applied magnetic field. Fig. 1(a) illustrates the nonlocal resistance change due to the switch of contact 4, which is represented by ΔR_{NL}. Unless specified otherwise, all measurement structures adhere to the configuration depicted in Fig. 1(a).

To explore how electrical currents affect the spin current in the inverted graphene spin valve, we first investigate the bias-dependent behavior of the spin signal by applying I_{Bias} to the spin injection circuit alongside with the AC current. Fig. 2(a) shows nonlocal resistance measurements across various bias currents, highlighting a significant spin signal reversal with increasing negative bias current. We used a three-probe geometry [41] to measure the contact resistance (R_C), obtaining a value of 5.5 $k\Omega$ for R_C, as illustrated in Fig. S1. At $I_{Bias} = 0\ \mu A$, the ΔR_{NL} measures around 5 Ω. Upon applying a positive current (30 μA), ΔR_{NL} increases to 9.5 Ω, representing a substantial 95 % amplification in the spin signal. Conversely, with a negative bias current, ΔR_{NL} diminishes and becomes negative at $I_{Bias} = -20\ \mu A$. At $I_{Bias} = -40\ \mu A$, ΔR_{NL} measures about −1.8 Ω, depicting a decrease of approximately −36 % compared to the zero bias current value.

In contrast to the response under bias current, the spin signal consistently shows a positive trend when an external DC current is applied. In Fig. 2(c), as the external current exceeds 50 μA, the spin signal nearly saturates, exhibiting a 100 % enhancement. Conversely, for $I_{Ext} < -50\ \mu A$, the spin signal is nearly suppressed below the noise level. The constant value of ΔR_{NL} for I_{Ext} large (or smaller) than 50 (-50) μA indicates the effective modulation of the spin signal by the external current. The spin signal enhancement under external current in our study is less pronounced than that reported in Ref. [30]. One possible explanation for this difference is the variation in device structure. In our IGSV, the drift current injector is positioned approximately 5 μm away from the spin detector electrode, whereas in Ref. [30], the separation is only about 0.9 μm. As a result, spins are more effectively directed within the drift field region, but outside this region, the spin decays exponentially [24,42].

The variations in the nonlocal spin signal with respect to applied

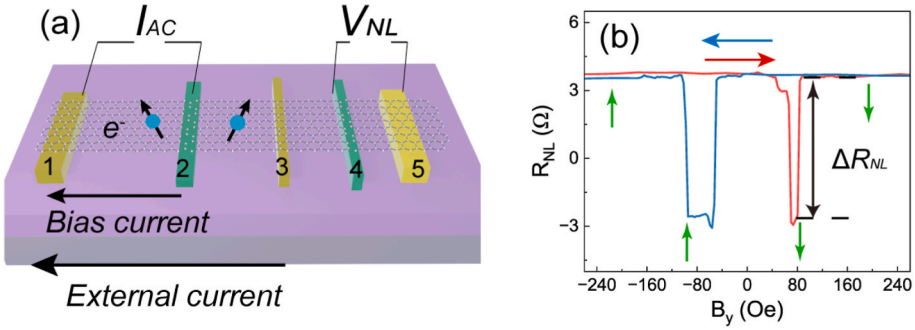

Fig. 1. The illustration of the device measurement setup. (a) The hBN/SLG stack is transferred onto the prepared electrodes. The gray color represents the Si substrate, while the purple color represents the SiO_2 layer. The green color represents the cobalt electrode, and the yellow color represents the Ti/Au electrode. The distance between the nearest electrode is about 3 μm. (b) The typical nonlocal resistance as a function of the in-plane magnetic field, without any external electrical current. (For interpretation of the references to color in this figure legend, the reader is referred to the Web version of this article.)

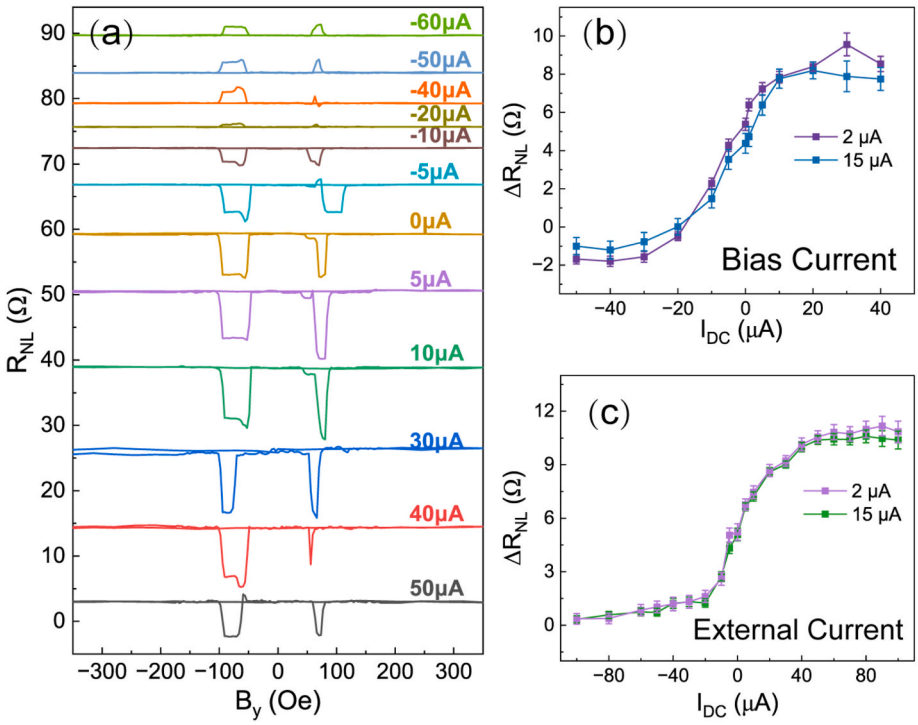

Fig. 2. The bias dependence of the nonlocal spin signals (a) Nonlocal resistance measured at different bias currents with an injection current of 2 μA. All curves are offset for clarity. The ΔR_{NL} varies based on both the (b) local bias current and (c) external DC current, considering injections current of 2 μA and 5 μA,respectively.

current show that in-plane current plays an important role in modulating the spin signal. However, the internal mechanisms of bias and external current differ. To further investigate the relationship between bias and external current effects on the spin signal, we studied the back gate voltage dependency of nonlocal spin transport measurements. Fig. 3(a) illustrates the modulation of the spin signal induced by the external current across different gate voltages. The graphene sheet resistance as function of the gate voltage is shown in Fig. S2, with the charge neutral point (CNP) located at approximately −30 V. To compare the spin signal at various gate voltages, we normalize ΔR_{NL} by its zero-current value, $\Delta R_{NL}(0)$. We observed diverse behaviors in the spin signal under external current across varying gate voltages. Notably, the extent to which the spin signal is influenced by the external current varies at various gate voltages. For instance, at $V_G = 40\ V$ with $I_{Ext} = 120\ \mu A$, the spin signal shows a 23 % increase compared to zero values. However, near the charge neutral point, at the $V_G = -30\ V$, the enhancement reaches up to 110 %. This contrasts with the non-monotonic enhancement reported in Ref. [30]. We attribute this difference to the uniform encapsulation of hBN and cleaner graphene in our IGSV, which ensures uniform mobility and reduces contamination throughout the device [43]. Conversely, in the hole-doped region ($V_G = -40\ V$), the spin signal behaves oppositely to that in the electron-doped region under external current. These findings indicate that spin diffusion in graphene is closely related to the type of charge carriers.

Understanding the spin drift effect induced by the electrical field is crucial for characterizing the relationship between electrical current and spin current in the inverted graphene-based spin valve. Carrier drift-diffusion modeling [24,31] emphasizes that when the drift velocity (expressed as $v_d = \mu E = \mu R_{sq} I_{DC}/w$, where w represents width of the channel) becomes comparable to the Fermi velocity, the spin drift field plays a pivotal role in spin transport [30,32]. The electron mobilities (μ) are derived as $\mu = 1/e \bullet \Delta\sigma/\Delta n$, where n represents carrier density and σ is the graphene conductance. Carrier density is calculated as $n = \alpha(V_G - V_{CNP})$, with α denoting the capacitive coupling constant set at $\alpha = 4.8 \times 10^{10}\ V^{-1}\ cm^{-2}$ [44]. In our work, near the CNP, we determined mobilities around about 8000 cm^2/Vs. Under these conditions, the drift

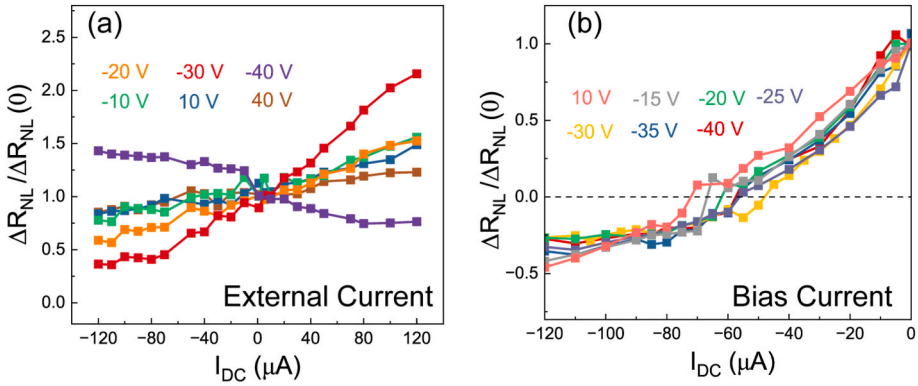

Fig. 3. The gate voltage dependence of nonlocal spin transport measurement. (a) External current dependence of the normalized spin signal concerning its zero-bias value at various gate voltages. (b) The bias current dependence of normalized spin signal variation across varying gate voltages.

velocity is compared to the Fermi velocity, leading to a noticeable modulation of the spin signal by the external current. Conversely, away from the CNP, the drift velocity decrease, resulting in a similar ratio of $\Delta R_{NL}/\Delta R_{NL}(0)$ without significant distinction.

The bias dependent of ΔR_{NL} shows no obvious variation under different carrier types, as shown in Fig. 3(b). However, all of the measured curves display an inverse trend in the spin signal. In our device, graphene is placed on the ferromagnetic electrodes, the interface between graphene and the contact will not change with the gate voltage due to the electrostatic shielding [22]. Comparatively, as illustrated in Fig. 1(a), the spin diffusion is more affected by the drift field induced by the external current, whereas bias current typically affects the spin signal through the spin injection process. The nonlinear bias dependence of the spin signal, especially the inversion of the spin signal, usually stems from changes in spin injection polarization. Gurram et al. [33] observed a notable shift in the spin signal attributed to bias current, linking the changes in nonlocal magnetic resistance primarily to modifications in spin-injection polarization. They assumed that the spin diffusion length remained unchanged due to the bias application between the injector contacts. Similarity, Leutenantsmeyer et al. [36], employing nonlocal spin transport alongside spin precession measurements, discovered that the spin signal variation occurred due to the changes in spin injection efficiency induced by bias current. Therefore, understanding the mechanism of sign-reversal at negative dc bias is crucial for unraveling the spin injection process in pinhole-dominant IGSV. Additionally, this understanding helps clarify the role of electrical current in the spin injection process.

Several mechanisms can contribute to the nonlinear bias-dependent spin signal. One significant factor is Joule heating, expressed as $P_{Joule} = R_{tun}I^2$, where R_{tun} represents contact resistance. The presence of narrower magnetic contacts (several microns) and thinner spin transport channels intensifies Joule heating [45]. These thermal effects arising from the bias current could potentially induce phenomena like thermoelectric spin voltage [46], or impact spin injection [47]. However, as illustrated in Fig. 2(b), at the same bias current ($-20\ \mu A$), a reversal in the spin signal is observed for $I_{2\ \mu A}$ while remaining positive for $I_{15\ \mu A}$. Additionally, if joule heating played a significant role in the nonlinear behaviour of the spin signal, we would expect to see more pronounced effects under external current conditions compared to bias current conditions. However, as shown in Fig. 2(c), the saturation of the spin signal under external current and bias current conditions occurs at similar current levels. Therefore, Joule heating is unlikely to be the cause of the observed spin signal reversal.

The energy-dependence electronic structure of the ferromagnetic electrode presents another possible mechanism for spin signal reversal. First-principles calculations from Ref. [48] suggest that the magnetic proximity effect at Co-graphene hybrid interfaces could contribute to spin signal reversal. It is worth noting that proximity effects between graphene and cobalt usually occur in 1D contacts. With the 2D contacts in our work, the Fermi level of graphene beneath the ferromagnetic electrode is strongly pinned and not effectively tunable by gate voltage [49,50]. Additionally, transfer curve indicating n-type doping (Fig. S2) suggests that charge transfer induced by the barrier layer is minimal [51]. Therefore the magnetic proximity effect might not be the reason governing the spin signal reversal. On the other hand, Zhu et al. [32] propose that the spin signal reversal is due to the spin-polarized electronic structure of the ferromagnetic electrodes. They propose a specific reverse bias voltage window capable of reversing the spin signal without relying on particular tunnel barrier conditions. However, this tunneling spin injection model assumes pinhole-free contacts, whereas our measured contact resistance is relatively low. The required DC bias voltage for signal reversal in our work does not align with the proposed bias window. For instance, before the breakdown of the barrier layer, the measured reverse bias voltage is approximately −110 mV. After the barrier layer breakdown, the reversal voltage increases significantly increase to about −350 mV. Therefore, this mechanism may not account for the nonlinear spin signal observed in our devices. However, this behavior indicates that the barrier layer plays an important role in spin signal reversal.

Daria et al. reported that tunnel barriers can become unstable, particularly at high currents, which may alter contact resistance and impact spin transport properties [52]. To explore this, we conducted additional three-terminal measurements with currents ranging from 5 to 100 μA. As shown in Fig. S3, the current-voltage characteristics of the contact resistance exhibit a nearly linear relationship, indicating pinhole-free contact behavior. However, under high current conditions, the *I–V* curve becomes less smooth, suggesting the formation of conductive nanofilaments within the barrier layer at high bias currents. Our experimental observations in Fig. 3(b) indicates that spin signals extracted near the CNP exhibit less reversal current and faster saturation compared to those away from the CNP. Conversely, away from the CNP, the reverse current increases. Since the contact is pinhole dominant, within the drift region (pinhole area), the significant electrical field enhances the impedance mismatch to a level where drift starts to dominate spin transport. This leads to a negative differential resistance and subsequent reversal of spin valve signals. Therefore, the drift current induced electrical field combined with the pinhole model may be one of the contributing factors. However, quantifying the pinhole area in the contact and the strength of the electrical field in the drift region remains challenging, beyond merely considering the contact resistance. Further theoretical and experimental investigations are essential to comprehensively understand the relationship between drift field and pinholes.

Unlike bias current, external current doesn't directly alter spin injection polarization since it doesn't directly apply to the injector. However, as depicted in Fig. 1(a), the injection circuit is influenced by the drift field generated by the external current. This influence is particularly noticeable for the pinhole contact, where the injection current from pinhole might be affected by the drift field. In earlier studies [24,30], the change in spin signal under external current was typically seen as an alteration of the spin diffusion length. However, the effect of external DC current on the interplay between spin injection and spin diffusion processes remains incompletely understood, particularly regarding its impact on spin injection polarization.

Indeed, Hanle precession measurements serve as an effective method to extract spin transport-related parameters, such as spin polarization and spin diffusion length (λ). When the magnetic field ($B_\perp$) is perpendicular to the device, it induces spins to precess from the injector towards the detector, influencing the spin signal through precession, relaxation, and dephasing as described by Eq. (1) [53,54]:

$$R_{NL} = \frac{p_i p_d D_S R_G}{W}\int_0^\infty \frac{1}{\sqrt{4\pi D_S t}} e^{-\frac{L^2}{4D_S t}} \cos(\omega_l t) e^{-\frac{t}{\tau_s}} dt, \quad (1)$$

Here, p_i and p_d are the spin polarizations for the injector and detector, respectively. W is the width of the graphene channel, R_G represent the graphene sheet resistance and L is the distance between injector and detector. D_S and τ_S are the spin diffusion coefficient and relaxation time. The Larmor frequency $\omega_l = \frac{g\mu_B}{\hbar}B_\perp$, Lande factor $g = 2$.

Hence, we conducted out-of-plane Hanle precession measurements to examine the correlation between spin transport parameters and the external current. Fig. 4(a) shows the Hanle precession measurement under an external current, with experimental data represented by half-filled dots and the fitting curve derived from Eq. (1) shown as a solid line. As the positive external current increases, the Hanle line width narrows, whereas under negative external current, the Hanle line width broadens. Although Eq. (1) does not explicitly include the drift term, it is well-established that a drift field can affect both the spin relaxation time and the spin diffusion constant [24,26,30], thereby altering the Hanle line width. It's noteworthy that, even in the presence of pinhole contacts, when both the resistance values of L and R ($R{=}W{\cdot}R_C/R_G$) [42]

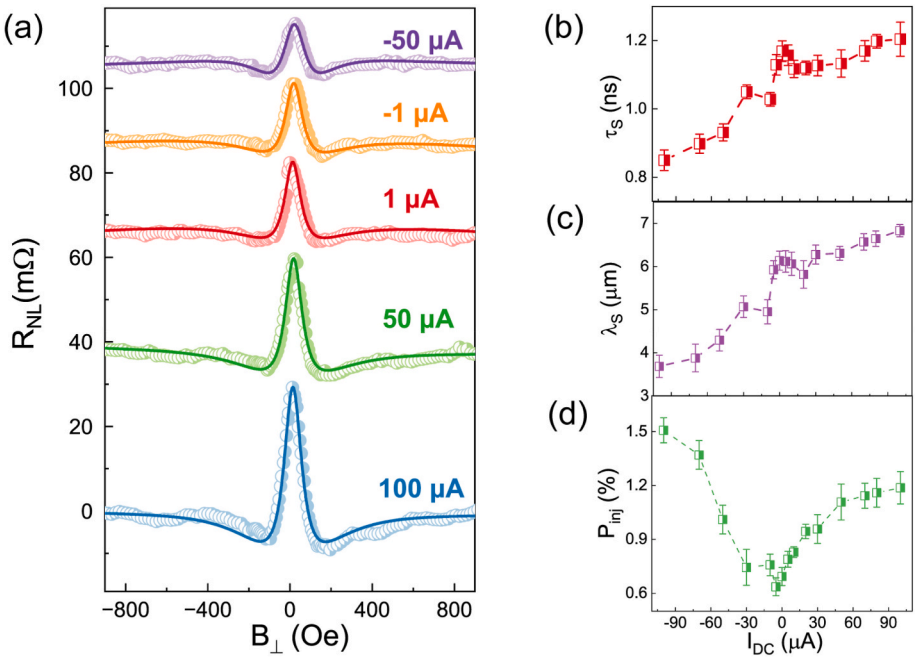

Fig. 4. The Hanle measurement dependent on external current. (a) The out-of-plane Hanle measurement is performed with different external DC current. The half-filled dot represents the experimental data and the line represents the fitting curve. All curves are offset for clarity. (b) The spin relaxation time τ_S, (c) the spin diffusion length λ_S and (d) the spin injection polarization as a function of external DC current.

surpass the spin diffusion length, the changes in the fitted Hanle curve's shape become relatively insignificant [55]. Consequently, data analysis employing Eq. (1) becomes feasible without the need to consider the impact of low-resistance contacts.

In Hanle fitting process, p_d remains fixed at a constant value of 0.6 % (at zero external DC current). This fixation occurs because the detector is positioned sufficiently far from the external electrical field. The justification of the Hanle fitting process is shown included in Fig. S7. These effects indirectly cause changes in the Hanle line width, as observed in our measurements. The spin transport-related parameter as function of external current is plotted in Fig. 4(b-d). The spin relaxation time is about 1.1 ns under zero external DC current, consistent with our previous work [15], suggesting that the nonmagnetic electrode does not introduce additional effects on spin transport. It is obvious that when a negative external current is applied, all spin diffusion-related parameters decrease, as shown in Fig. 4(b-c). This observed reduction in spin transport-related parameters (including D_S, as shown in Fig. S5) under negative external current is due to the influence of the drift field. The directional nature of the drift field governs the diffusion of spin current toward the detector electrode under negative external current. As the positive external current increases, the drift velocity (v_d), which is directly proportional to the external current, also rises, potentially leading to a corresponding increase in the spin diffusion constant. We have also studied the charge diffusion constant D_c in Fig. S6, which exhibits a trend comparable to that of the spin diffusion constant [56–58]. This highlights the crucial role of the spin drift field in spin transport and results in enhanced diffusion of the spin current toward the detector [24,30].

Fig. 4(d) illustrates the relationship between the efficiency of spin-injection polarization (P_{inj}) and external current. Notably, P_{inj} is not constant with respect to external current but rather nearly symmetric around zero external electrical current. These results suggest that the effective spin polarization changes with the strength of the drift field rather than its direction. To delve deeper into the underlying physical mechanisms, we further studied the interface between graphene and the injector under an external current field, as shown in Fig. S4. When an external current is applied, we observe a shift in the current-voltage curve that aligns with the direction of the external current field. Moreover, as the absolute value of the external current increases, the output curve becomes non-linear. This behavior can be attributed to the multiple injection points at the interface between the graphene and the electrode, given the pinhole contact characteristics of our device [16]. At low external current levels, while the external current field influences the distribution of carriers, they remain relatively stable during current-voltage measurements, resulting in a linear *I–V* curve. However, as the external current increases, carriers injected from the pinhole contacts are significantly affected by the drift field, which can cause local measurement voltage instabilities, leading to a less smooth output curve. When carriers are injected, a negative drift field causes an increase in voltage, while a positive drift field causes a decrease, resulting in changes in contact resistance (as shown in Fig. S4b). In nonlocal spin transport measurements, when spin is injected from the injection point, the drift field causes carriers to move away from these points, this modified barrier carrier distribution, which effectively reduces spin backflow and spin-flip scattering [26,52,59]. As a result, the efficiency of spin injection increases with the applied external DC current, regardless of its direction. Thus, we find that the external current not only plays a crucial role in spin current diffusion but also in the creation of the spin current.

4. Conclusion

In summary, we investigated the effect of electrical currents, encompassing both bias and external currents, on spin current in an inverted graphene-based spin valve. Our study revealed substantial influences of these currents not only on spin current diffusion but also on the generation of the spin current. Particularly noteworthy was the distinct tunability of the spin signal under external current across various gate voltages, emphasizing the significant role of the spin drift effect in our device. Hanle precession measurements confirmed this observation and demonstrated that the spin drift field enhances effective spin polarization in pinhole contacts. These findings provide evidence for the nonlinear bias-dependent spin signal reversal at different gate voltages. We considered several mechanisms, including joule heating,

the energy-dependence electronic structure of the ferromagnetic electrode, and the drift field effect, to explain this spin signal reversal. By comparing these mechanisms with our experimental data, we concluded that the drift field, combined with the pinhole contact model, predominantly drives the bias-dependent spin signal reversal. These findings highlight the relationship between bias and external currents in their impact on the spin signal. This research not only enriches the understanding of electrically tunable spin current but also paving the way for the application of future graphene-based spintronic devices.

CRediT authorship contribution statement

Jian Zhou: Writing – original draft, Formal analysis, Data curation. **Xianyang Lu:** Supervision, Formal analysis. **Bing Zhao:** Writing – review & editing, Supervision. **Jiaju Yang:** Formal analysis. **Yu Yan:** Formal analysis. **Jing Wu:** Formal analysis. **Yong Pu:** Formal analysis. **Rong Zhang:** Supervision, Formal analysis. **Yongbing Xu:** Writing – review & editing, Supervision, Funding acquisition.

Data availability

All data are available in the main text.

Declaration of competing interest

The authors declare that they have no known competing financial interests or personal relationships that could have appeared to influence the work reported in this paper.

Acknowledgements

This work is supported by the National Natural Science Foundation of China (Grant Nos. 12104216, 12241403 and 61427812), and the Natural Science Foundation of Jiangsu Province of China (Nos. BK20200307, BK20192006, and BK20180056), and Postgraduate Research & Practice Innovation Program of Jiangsu Province (KYCX21_0051).

Appendix A. Supplementary data

Supplementary data to this article can be found online at https://doi.org/10.1016/j.carbon.2025.120140.

References

[1] X. Lin, W. Yang, K.L. Wang, W. Zhao, Two-dimensional spintronics for low-power electronics, Nat. Electron. 2 (7) (2019) 274–283.
[2] V.H. Guarochico-Moreira, J.L. Sambricio, K. Omari, C.R. Anderson, D.A. Bandurin, J.C. Toscano-Figueroa, N. Natera-Cordero, K. Watanabe, T. Taniguchi, I. V. Grigorieva, I.J. Vera-Marun, Tunable spin injection in high-quality graphene with one-dimensional contacts, Nano Lett. 22 (3) (2022) 935–941.
[3] J. Panda, M. Ramu, O. Karis, T. Sarkar, M.V. Kamalakar, Ultimate spin currents in commercial chemical vapor deposited graphene, ACS Nano 14 (10) (2020) 12771–12780.
[4] I. Žutić, J. Fabian, S. Das Sarma, Spintronics: fundamentals and applications, Rev. Mod. Phys. 76 (2) (2004) 323–410.
[5] W. Han, R.K. Kawakami, M. Gmitra, J. Fabian, Graphene spintronics, Nat. Nanotechnol. 9 (10) (2014) 794–807.
[6] A. Manchon, H.C. Koo, J. Nitta, S.M. Frolov, R.A. Duine, New perspectives for Rashba spin-orbit coupling, Nat. Mater. 14 (9) (2015) 871–882.
[7] M. Johnson, R.H. Silsbee, Interfacial charge-spin coupling: injection and detection of spin magnetization in metals, Phys. Rev. Lett. 55 (17) (1985) 1790–1793.
[8] F.L. Bakker, A. Slachter, J.P. Adam, B.J. van Wees, Interplay of Peltier and Seebeck effects in nanoscale nonlocal spin valves, Phys. Rev. Lett. 105 (13) (2010) 136601.
[9] S.Q. Shen, Spin transverse force on spin current in an electric field, Phys. Rev. Lett. 95 (18) (2005) 187203.
[10] T. Liu, G. Vignale, Electric control of spin currents and spin-wave logic, Phys. Rev. Lett. 106 (24) (2011) 247203.
[11] X. He, C. Zhang, D. Zheng, P. Li, J.Q. Xiao, X. Zhang, Nonlocal Spin Valves Based on Graphene/Fe(3)GeTe(2) van der Waals Heterostructures, ACS Appl. Mater. Interfaces 15 (7) (2023) 9649–9655.
[12] R. Jansen, A. Spiesser, Y. Fujita, H. Saito, S. Yamada, K. Hamaya, S. Yuasa, Superimposed contributions to two-terminal and nonlocal spin signals in lateral spin-transport devices, Phys. Rev. B 104 (14) (2021) 144419.
[13] D. Khokhriakov, B. Karpiak, A.M. Hoque, B. Zhao, S. Parui, S.P. Dash, Robust spin interconnect with isotropic spin dynamics in chemical vapor deposited graphene layers and boundaries, ACS Nano 14 (11) (2020) 15864–15873.
[14] Z.G. Yu, M.E. Flatté, Spin diffusion and injection in semiconductor structures: electric field effects, Phys. Rev. B 66 (23) (2002).
[15] J. Zhou, X. Lu, J. Yang, X. Zhang, Q. Liu, Q. Zeng, Y. Yan, Y. Li, L. Wei, J. Wu, Y. Pu, R. Liu, L. He, R. Zhang, Y. Xu, Intrinsic spin transport properties observed in contamination-free graphene-based spin valve, Carbon 228 (2024) 119321.
[16] M. Drogeler, C. Franzen, F. Volmer, T. Pohlmann, L. Banszerus, M. Wolter, K. Watanabe, T. Taniguchi, C. Stampfer, B. Beschoten, Spin lifetimes exceeding 12 ns in graphene nonlocal spin valve devices, Nano Lett. 16 (6) (2016) 3533–3539.
[17] A. Dankert, M.V. Kamalakar, J. Bergsten, S.P. Dash, Spin transport and precession in graphene measured by nonlocal and three-terminal methods, Appl. Phys. Lett. 104 (19) (2014) 192403.
[18] G. Stecklein, P.A. Crowell, J. Li, Y. Anugrah, Q. Su, S.J. Koester, Contact-induced spin relaxation in graphene nonlocal spin valves, Phys. Rev. Appl. 6 (5) (2016) 054015.
[19] H. Dery, H. Wu, B. Ciftcioglu, M. Huang, Y. Song, R. Kawakami, J. Shi, I. Krivorotov, I. Zutic, L.J. Sham, Nanospintronics based on magnetologic gates, IEEE. Trans. Electron. Dev. 59 (1) (2012) 259–262.
[20] H. Wen, H. Dery, W. Amamou, T. Zhu, Z. Lin, J. Shi, I. Žutić, I. Krivorotov, L. J. Sham, R.K. Kawakami, Experimental demonstration of xor operation in graphene magnetologic gates at room temperature, Phys. Rev. Appl. 5 (4) (2016).
[21] D. Khokhriakov, B. Karpiak, A.M. Hoque, S.P. Dash, Two-dimensional spintronic circuit architectures on large scale graphene, Carbon 161 (2020) 892–899.
[22] T. Bisswanger, Z. Winter, A. Schmidt, F. Volmer, K. Watanabe, T. Taniguchi, C. Stampfer, B. Beschoten, CVD bilayer graphene spin valves with 26 mum spin diffusion length at room temperature, Nano Lett. 22 (12) (2022) 4949–4955.
[23] D. Khokhriakov, S. Sayed, A.M. Hoque, B. Karpiak, B. Zhao, S. Datta, S.P. Dash, Multifunctional spin logic operations in graphene spin circuits, Phys. Rev. Appl. 18 (6) (2022) 064063.
[24] C. Jozsa, M. Popinciuc, N. Tombros, H.T. Jonkman, B.J. van Wees, Electronic spin drift in graphene field-effect transistors, Phys. Rev. Lett. 100 (23) (2008) 236603.
[25] W. Han, W.H. Wang, K. Pi, K.M. McCreary, W. Bao, Y. Li, F. Miao, C.N. Lau, R. K. Kawakami, Electron-hole asymmetry of spin injection and transport in single-layer graphene, Phys. Rev. Lett. 102 (13) (2009) 137205.
[26] C. Józsa, M. Popinciuc, N. Tombros, H.T. Jonkman, B.J. van Wees, Controlling the efficiency of spin injection into graphene by carrier drift, Phys. Rev. B 79 (8) (2009) 081402 (R).
[27] M.V. Kamalakar, A. Dankert, P.J. Kelly, S.P. Dash, Inversion of Spin Signal and Spin Filtering in Ferromagnet|Hexagonal Boron Nitride-Graphene van der Waals Heterostructures, Sci. Rep. 6 (2016) 21168.
[28] J. Ingla-Aynés, A.A. Kaverzin, B.J. van Wees, Carrier drift control of spin currents in graphene-based spin-current demultiplexers, Phys. Rev. Appl. 10 (4) (2018).
[29] X. He, Y. Wen, C. Zhang, P. Li, D. Zheng, A. Chen, A. Manchon, X. Zhang, Spin transport in multilayer graphene away from the charge neutrality point, Carbon 172 (2021) 474–479.
[30] J. Ingla-Aynes, R.J. Meijerink, B.J. Wees, Eighty-eight percent directional guiding of spin currents with 90 mum relaxation length in bilayer graphene using carrier drift, Nano Lett. 16 (8) (2016) 4825–4830.
[31] Z.G. Yu, M.E. Flatté, Electric-field dependent spin diffusion and spin injection into semiconductors, Phys. Rev. B 66 (20) (2002).
[32] T. Zhu, S. Singh, J. Katoch, H. Wen, K. Belashchenko, I. Žutić, R.K. Kawakami, Probing tunneling spin injection into graphene via bias dependence, Phys. Rev. B 98 (5) (2018) 054412.
[33] M. Gurram, S. Omar, B.J.V. Wees, Bias induced up to 100% spin-injection and detection polarizations in ferromagnet/bilayer-hBN/graphene/hBN heterostructures, Nat. Commun. 8 (1) (2017) 248.
[34] Y. Fujita, M. Yamada, M. Tsukahara, T. Naito, S. Yamada, K. Sawano, K. Hamaya, Nonmonotonic bias dependence of local spin accumulation signals in ferromagnet/semiconductor lateral spin-valve devices, Phys. Rev. B 100 (2) (2019).
[35] M.V. Kamalakar, A. Dankert, J. Bergsten, T. Ive, S.P. Dash, Enhanced tunnel spin injection into graphene using chemical vapor deposited hexagonal boron nitride, Sci. Rep. 4 (2014) 6146.
[36] J.C. Leutenantsmeyer, T. Liu, M. Gurram, A.A. Kaverzin, B.J. van Wees, Bias-dependent spin injection into graphene on YIG through bilayer hBN tunnel barriers, Phys. Rev. B 98 (12) (2018).
[37] W. Han, K.M. McCreary, K. Pi, W.H. Wang, Y. Li, H. Wen, J.R. Chen, R. K. Kawakami, Spin transport and relaxation in graphene, J. Magn. Magn Mater. 324 (4) (2012) 369–381.
[38] F.J. Jedema, H.B. Heersche, A.T. Filip, J.J.A. Baselmans, B.J. van Wees, Electrical detection of spin precession in a metallic mesoscopic spin valve, Nature 416 (6882) (2002) 713–716.
[39] X. Lou, C. Adelmann, S.A. Crooker, E.S. Garlid, J. Zhang, K.S.M. Reddy, S. D. Flexner, C.J. Palmstrøm, P.A. Crowell, Electrical detection of spin transport in lateral ferromagnet–semiconductor devices, Nat. Phys. 3 (3) (2007) 197–202.
[40] W. Amamou, G. Stecklein, S.J. Koester, P.A. Crowell, R.K. Kawakami, Spin absorption by in situ deposited nanoscale magnets on graphene spin valves, Phys. Rev. Appl. 10 (4) (2018).
[41] F. Volmer, M. Drogeler, E. Maynicke, N. von den Driesch, M.L. Boschen, G. Guntherodt, B. Beschoten, Role of MgO barriers for spin and charge transport in Co/MgO/graphene nonlocal spin-valve devices, Phys. Rev. B 88 (16) (2013) 161405.

[42] M. Popinciuc, C. Józsa, P.J. Zomer, N. Tombros, A. Veligura, H.T. Jonkman, B. J. van Wees, Electronic spin transport in graphene field-effect transistors, Phys. Rev. B 80 (21) (2009) 214427.
[43] L. Wang, I. Meric, P.Y. Huang, Q. Gao, Y. Gao, H. Tran, T. Taniguchi, K. Watanabe, L.M. Campos, D.A. Muller, J. Guo, P. Kim, J. Hone, K.L. Shepard, C.R. Dean, One-dimensional electrical contact to a two-dimensional material, Science 342 (6158) (2013) 614–617.
[44] M. Drogeler, F. Volmer, M. Wolter, B. Terres, K. Watanabe, T. Taniguchi, G. Guntherodt, C. Stampfer, B. Beschoten, Nanosecond spin lifetimes in single- and few-layer graphene-hBN heterostructures at room temperature, Nano Lett. 14 (11) (2014) 6050–6055.
[45] R. Jansen, A. Spiesser, S. Yuasa, Magnetic control of heat generation in a magnetic tunnel contact with spin accumulation, Phys. Rev. B 106 (18) (2022).
[46] J.F. Sierra, I. Neumann, J. Cuppens, B. Raes, M.V. Costache, S.O. Valenzuela, Thermoelectric spin voltage in graphene, Nat. Nanotechnol. 13 (2) (2018) 107–111.
[47] A. Slachter, F.L. Bakker, J.P. Adam, B.J. van Wees, Thermally driven spin injection from a ferromagnet into a non-magnetic metal, Nat. Phys. 6 (11) (2010) 879–882.
[48] B. Zhao, D. Khokhriakov, B. Karpiak, A.M. Hoque, L. Xu, L. Shen, Y.P. Feng, X. Xu, Y. Jiang, S.P. Dash, Electrically controlled spin-switch and evolution of Hanle spin precession in graphene, 2D Mater. 6 (3) (2019).
[49] J. Xu, S. Singh, J. Katoch, G. Wu, T. Zhu, I. Zutic, R.K. Kawakami, Spin inversion in graphene spin valves by gate-tunable magnetic proximity effect at one-dimensional contacts, Nat. Commun. 9 (1) (2018) 2869.
[50] P. Lazić, K.D. Belashchenko, I. Žutić, Effective gating and tunable magnetic proximity effects in two-dimensional heterostructures, Phys. Rev. B 93 (24) (2016) 241401(R).
[51] D. Belotcerkovtceva, R.P. Maciel, E. Berggren, R. Maddu, T. Sarkar, Y.O. Kvashnin, D. Thonig, A. Lindblad, O. Eriksson, M.V. Kamalakar, Insights and implications of intricate surface charge transfer and sp3-defects in graphene/metal oxide interfaces, ACS Appl. Mater. Interfaces 14 (31) (2022) 36209–36216.
[52] D. Belotcerkovtceva, J. Panda, M. Ramu, T. Sarkar, U. Noumbe, M.V. Kamalakar, High current limits in chemical vapor deposited graphene spintronic devices, Nano Res. 16 (4) (2022) 4233–4239.
[53] A. Dankert, S.P. Dash, Electrical gate control of spin current in van der Waals heterostructures at room temperature, Nat. Commun. 8 (2017) 16093.
[54] B. Zhao, X. Xu, L. Wang, J. Li, Z. Zhang, P. Liu, Q. Liu, Z. Wang, Y. Jiang, Effect of Ti doping on spin injection and relaxation in few-layer graphene, Carbon 127 (2018) 568–575.
[55] T. Maassen, I.J. Vera-Marun, M.H.D. Guimarães, B.J. van Wees, Contact-induced spin relaxation in Hanle spin precession measurements, Phys. Rev. B 86 (23) (2012) 235408.
[56] C. Józsa, T. Maassen, M. Popinciuc, P.J. Zomer, A. Veligura, H.T. Jonkman, B. J. van Wees, Linear scaling between momentum and spin scattering in graphene, Phys. Rev. B 80 (24) (2009).
[57] I.G. Serrano, J. Panda, F. Denoel, Ö. Vallin, D. Phuyal, O. Karis, M.V. Kamalakar, Two-Dimensional flexible high diffusive spin circuits, Nano. Letter. 19 (2) (2019) 666–673.
[58] P.R. Whelan, Q. Shen, B. Zhou, I.G. Serrano, M.V. Kamalakar, D.M.A. Mackenzie, J. Ji, D. Huang, H. Shi, D. Luo, M. Wang, R.S. Ruoff, A.-P. Jauho, P.U. Jepsen, P. Bøggild, J.M. Caridad, Fermi velocity renormalization in graphene probed by terahertz time-domain spectroscopy, 2D Mater. 7 (3) (2020).
[59] S. Zhang, P.M. Levy, A.C. Marley, S.S.P. Parkin, Quenching of magnetoresistance by hot electrons in magnetic tunnel junctions, Phys. Rev. Lett. 79 (19) (1997) 3744–3747.